SI Appendix for

A Specialized Metabolic Pathway Partitions Citrate in Hydroxyapatite to Impact Mineralization of Bones and Teeth

Naomi Dirckx[1,2*], Qian Zhang[1,3], Emily Y Chu[4,5], Robert J Tower[1], Zhu Li[1,2], Shenghao Guo[6], Shichen Yuan[7], Pratik A Khare[8], Cissy Zhang[9], Angela Verardo[1], Lucy O. Alejandro[5], Angelina Park[4], Marie-Claude Faugere[10], Stephen L Helfand[11], Martha J Somerman[5], Ryan C Riddle[1,2,12], Rafael de Cabo[13], Anne Le[9], Klaus Schmidt-Rohr[7], and Thomas L Clemens[1,2,12*]

[1]Department of Orthopaedic Surgery, Johns Hopkins University School of Medicine, Baltimore, MD, USA
[2]Department of Orthopaedics, University of Maryland School of Medicine, Baltimore, MD 21201, USA.
[3]Department of Nutrition and Health, China Agricultural University, Beijing 100193, China
[4]Department of General Dentistry, Operative Division, University of Maryland School of Dentistry Baltimore, MD, USA
[5]National Institute of Arthritis and Musculoskeletal and Skin Diseases (NIAMS), National Institutes of Health (NIH), Bethesda, MD, USA
[6]Department of Biomedical Engineering, Johns Hopkins University Whiting School of Engineering, Baltimore, MD, USA
[7]Department of Chemistry, Brandeis University, Waltham, MA USA
[8]Department of Chemical and Biomolecular Engineering, Johns Hopkins University, Baltimore, MD USA
[9]Department of Pathology and Oncology, Johns Hopkins University School of Medicine, Baltimore, MD USA
[10]Department of Medicine, University of Kentucky, Lexington, Kentucky, USA.
[11]Department of Molecular Biology, Cell Biology and Biochemistry, Brown University, Providence, RI USA
[12]The Baltimore Veterans Administration Medical Center, Baltimore, MD USA
[13]Translational Gerontology Branch. National Institute on Aging, National Institutes of Health, Baltimore, MD USA

*Corresponding authors:

Email: tclemens@som.umaryland.edu (TLC), dirckxnaomi@gmail.com (ND)

Materials and Methods

Animals

The *Slc13a5*$^{-/-}$(1) and *Slc13a5* floxed mice, both in C57BL/6 background, were generously provided by Dr. Rafael De Cabo (NIA, Baltimore). For the global *Slc13a5*$^{-/-}$ mice, breeding pairs were set up by mating heterozygous males and females. In the skeletal-specific knockout model, the *Slc13a5* gene was recombined in osteoblasts (from embryonic day 17 onward) by crossing osteocalcin (*Oc*)-*Cre*(2) mice with *Slc13a5* floxed mice. Matings were set up between male *Oc-Cre*$^{+/-}$;*Slc13a5*$^{lox/lox}$ and female *Oc-Cre*$^{-/-}$;*Slc13a5*$^{lox/lox}$ to obtain progeny including *Slc13a5* conditional knockout (cKO) (*Oc-Cre*$^{+/-}$;*Slc13a5*$^{lox/lox}$ and further referred to as *Slc13a5*^{cKO}) mice and littermate controls (*Oc-Cre*$^{-/-}$;*Slc13a5*$^{lox/lox}$). Zinc transporter (*Zip1*) KO mice were generated in our lab with the support of NINDS JHU Center for Neuroscience Research, Murine Mutagenesis Core (NS050274), using the CRISPR/Cas9 technique which caused a 171bp insertion that induced a frameshift and a premature stop codon (TAA) in exon 2. Briefly, from the 4 exons in the ZIP 1 gene (SLC39A1), the start codon ATG is located in exon 2. The sgRNA (GCGCCCAGAAGCAGTCGCATCGG) in the corresponding exon 2 of the mouse *Zip1* gene was designed with CGG, Protospacer Adjacent Motif (PAM), at the end, and was transcribed and purified. The DNA fragment consisting of target sequence and "scaffold" sequence was generated with PCR and amplified in a plasmid. The DNA fragment and sgRNA were suspended in the injection buffer combined with Cas9 mRNA. 250 embryos were injected before being transferred into recipient female mice. 50 pups were born after 3 weeks of gestation. The pups were screened for potential ZIP1 gene knockout. The PCR and sequencing covered the whole exon 2 and partial intron 1 and intron 2. Pups with 171 bps insertion in exon 2 causing frame shift and premature stop codon were identified. The identified mice were crossed with C57BL/6 mice before they were crossed again with their heterozygous offspring to generate homozygous pups. The deletion of ZIP1 protein from knockout mouse was confirmed by Western Blot. *Slc13a5*$^{-/-}$;*Zip1*$^{-/-}$ dKO, control and single KO littermates were generated by crossing *Slc13a5*$^{+/-}$;*Zip1*$^{+/-}$ double heterozygote

males and females. mTmG mice (B6.129(Cg)-Gt(ROSA)26Sor$^{tm4(ACTB-tdTomato,-EGFP)Luo}$/J) were purchased from The Jackson Laboratory.

Genotyping was performed on tail biopsies or ear punches using the following primers for *Slc13a5* KO allele: NADC5 loxF3 *GACTTAGCACAGCAGGTACT*, NADC5 frtR2 *GATCACTGTGATCTGGCCTA*, and for WT allele: NADC5 loxF3 *GACTTAGCACAGCAGGTACT,* NADC5 loxR TTACCAACCACCTCGCTAGT; ZIP1 FW *CCCACCCATGCTAGTTTTCTCTGTATAGGTCC*, ZIP1 RV *GCCCAACCTCCGAAGCAGAAAAGACTCACCTG*, Cre FW *GAA CCT GAT GGA CAT GTT CAG G*, Cre RV *AGT GCG TTC GAA CGC TAG AGC CTG T;* mTmG common primer *CTT TAA GCC TGC CCA GAA GA;* mTmG mutant FW *TAG AGC TTG CGG AAC CCT TC;* Wild Type FW *AGG GAG CTG CAG TGG AGT AG*

Animals were euthanized by isoflurane inhalation and subsequent cervical dislocation.

Serum analysis

Serum citrate levels were measured using a commercially available colorimetric assay (Millipore Sigma)

High-resolution micro-computed tomographic imaging (micro-CT)

For mineralized tissue analysis, an ex vivo micro-computed tomography (micro-CT) imaging system (Skyscan 1275 CT, Bruker, Kontich, Belgium) with corresponding Skyscan software was used. For ex vivo long bone analysis, 65 kV, 153 μA, 160ms exposure time, 10 μm voxel size resolution and a 0.5 mm Al filter were used as scanning parameters.). For tooth analysis, mandibles were scanned with 70 kV, 142 μA, 200ms exposure time, 6.7 μm voxel size resolution and a 0.5 mm Al filter as scanning parameters. Samples were reconstructed using the Nrecon software (Bruker) with 20% beam hardening correction, ring artifact correction of 5 and CS to Image conversion was 0-0.05 for long bones and 0-0.09 for teeth. 3D reconstructed images were generated using CTVol software (Bruker). The ex vivo micro-CT analysis of the femur included both trabecular and cortical bone analyses and was performed using CTAn (Bruker). For trabecular bone quantification, a region of interest

containing 100 slices (1 mm) was chosen 50 slices (500 μm) below the growth plate. For cortical analysis, a region of interest containing 50 slices (500 μm) from the midpoint of the femur, 250 μm towards the proximal end and 250 μm towards the distal end. Bone volume/tissue volume (BV/TV, %), trabecular number (Tb.N, 1/mm), trabecular separation (Tb.Sp, mm), trabecular thickness (Tb.Th, mm), and cortical thickness (Cort. Th, mm) were determined using CTAn software (Bruker). For tooth analysis, 3D segmentation was performed in 3D slicer(3). Briefly, enamel, dentin, cementum and pulp were defined by thresholding within a respective intensity range (enamel > 2000 mg/cm^3 HA; dentin 1000-1500 mg/cm^3 HA; cementum 650 – 1000 mg/cm^3 HA; pulp <300 mg/cm^3 HA) and individual compartments from molar 1 (M1) were manually segmented to obtain their respective volumes and density.

Exfoliated primary teeth from male children were scanned in a Sanco micro-CT 50 scanner (Scanco Medical, Bassersdorf, Switzerland) at 70 kVp, 76 μA, 0.5 Al filter, 900 ms integration time, and 10 μm voxel dimension. DICOM files were created and exported from scan data. Reconstructed images were loaded and analyzed in AnalyzePro 1.0 (AnalyzeDirect, Overland Park, KS). Images were oriented anatomically using the incisal edge, mesial/distal, and facial/lingual heights of contour to locate the long axis of the tooth. To determine mineral densities, oriented scans were calibrated to a standard curve of five known hydroxyapatite (HA) densities (mg/cm^3 HA). Enamel was segmented at 1500 mg/cm^3 HA, and dentin was segmented at 650-1499 mg/cm^3 HA. Thickness was determined using cortical thickness algorithms from the apical 100 slices from the pulp horn forming a hollow cylinder.

Whole bone biomechanical testing

A low force mechanical testing system (Bose Electroforce) was used to assess the biomechanical properties of excised bone. After specimens were thawed to room temperature in a calcium-buffered saline bath, the mechanical properties of the femoral midshaft were assessed by 3-point bending by applying a flexion moment in the anterior-posterior plane. The force was applied at a constant displacement rate (0.03 mm/sec) and the obtained force-displacement data was used to determine

yield load, failure load, stiffness, work-to-failure, and post-yield displacement. The material properties (elastic modulus, ultimate strength, and modulus of toughness) were obtained by adjusting the force-displacement data for the appropriate femoral mid-shaft area moment of inertia, as measured by micro-CT.

Slc13a5 Immunohistochemistry

Paraffin section from 2 week old mouse teeth were used for SLC13A5 staining using anti-SLC13A5 antibodies (Invitrogen, PA5-113058) and the VECTASTAIN® ELITE® ABC-HRP Kit, Peroxidase (Rabbit IgG), according to the manufacturer's protocol. Substrate reaction was visualized with AEC Peroxidase (HRP) Substrate kit (LSBio). Sections were counterstained with Harris Hematoxylin.

Quantitative histomorphometry

For histomorphometric purposes, bones were fixed in 4% PFA (overnight at 4°C) and subsequently immersed in 100% ethanol before embedding in methyl methacrylate (MMA) without decalcification. Five µm deplasticized sections were cut on a Jung 2065 Supercut microtome and mounted on coated slides. Slides were stained with toluidine blue for static histomorphometry to quantify osteoblast and osteoclast number and surface. For dynamic histomorphometry, assessing mineral apposition rate (MAR) and bone formation rate (BFR), 10-week old mice were double labeled with calcein (10 mg/kg BW, Sigma) and Alizarin Red (30 mg/kg BW, Sigma) 3 and 8 days prior to euthanizing, respectively by intraperitoneal injection. Histomorphometric analyses were performed using a semiautomatic method (Osteoplan II, Kontron Instruments Ltd.). Histomorphometric parameters followed the recommended nomenclature of the American Society of Bone and Mineral Research(4). For the trabecular bone analysis, a region of interest (ROI) was selected and delineated into 2-mm segments along the longitudinal direction. The vertical distance between the first image in the ROI and the growth plate was 0.5 mm.

Lineage tracing

Oc-Cre;mTmG pups were sacrificed at postnatal (P) day 7 and the jaws including the teeth were fixated in 4% PFA overnight. Jaws and teeth were decalcified for 1 week with 14% EDTA while shaking. Subsequently, jaws were washed in PBS and submerged in 30% sucrose in PBS overnight before embedding in OCT compound (Sakura). Cyrosections were made with a 5 µm thickness and imaged and imaged with a fluorescent microscope (Nikon Eclipse Ci).

^{13}C Solid-state NMR

Bone chip/teeth collection and preparation: 6 week old control and *Slc13a5*$^{-/-}$ mice were injected with ^{13}C-glucose (2 g/kg BW) daily for one week and sacrificed subsequently. For the rescue experiment with *Zip1* deletion, bones were collected and ^{13}C citrate was determined without ^{13}C-glucose enrichment. Cortical bone chips from 2 tibiae and 2 femurs were collected by removing the epiphysis and growth plate and depleting the bone marrow by centrifugation. Bones from multiple mice were pooled to obtain a total amount of 86-100 mg of bone chips per sample and packed into 4-mm zirconia NMR rotors with Kel-F® caps. All molars from the mandibula were extracted from 12 week old mice and all 6 molars from one mouse were pooled to one sample.

Solid state NMR spectroscopy: The solid-state NMR experiments were performed using a Bruker Neo 400WB spectrometer at 100 MHz for ^{13}C in a Bruker 4-mm double-resonance magic-angle spinning probe head at a spinning frequency of 8 kHz with high-power ($\gamma B_1/2\pi$ = 85 kHz) proton decoupling. Cross-polarization (CP) MAS ^{13}C NMR experiments were performed with a contact time of 1.1 ms and a 90-100% amplitude ramp on the ^{1}H channel. The recycle delays were 2–4 s depending on the specific ^{1}H spin-lattice relaxation time of the sample. The total measurement time was 10–12 h per spectrum. The total signal per transient recorded is proportional to the amount of organics. The amount of citrate was determined by integration of the 76-ppm peak. Signals of carbons with weak C—H dipolar couplings were selected by 40 us of gated decoupling before signal detection. The 76-

ppm peak of the C-OH carbon of citrate, which is not bonded to hydrogen, was retained selectively, which resolved potential overlap with carbohydrate signals.

Single cell sequencing analysis

Cells derived from the endosteal bone marrow region (GSE145477, PMID: 32286228) were analyzed in Seurat, with mesenchymal lineage cells subsequently subset according to previous author's analyses. Mesenchymal lineage cells were subjected to trajectory analysis using Monocle, with the stem, osteogenic and adipogenic branches identified by marker gene expression of Cd34, Bglap and Adipoq, respectively. Pseudotime was assigned using the Cd34 expressing branch as the root state. Deviation in gene expression of indicated genes were shown across the established pseudotime axis.

Isolation of primary calvarial osteoblasts

For the isolation of primary calvaria-derived osteoblasts (pCOBs), calvaria from newborn pups were carefully isolated, very briefly rinsed in 70% ethanol, thoroughly washed in sterile PBS and temporarily stored in α-MEM (Corning) without FBS until digest in 50 ml tubes. Primary osteoblasts were isolated using 1.8 mg/ml collagenase type I (Worthington Biochemical Corp. Cat no 4197) in 5 consecutive digest steps performed at 37°C with shaking. The first 2 digests obtained by 10 minutes of moderate shaking were discarded. The following 3 digests with 15 minutes of moderate shaking were collected in α-MEM (α-MEM, Corning) with 10% FBS to neutralize enzyme activity. After overnight incubation, non-adherent cells were removed by washing and the culture medium was replaced. The cells were cultured in α-MEM supplemented with 10% FBS, and antibiotics (1%, penicillin 50 units/ml and streptomycin 50 μg/ml) (GIBCO). All experiments were performed in passage 1 or 2. pCOBs were treated with 5μM of SLC13A5 inhibitor PF-06761281 (Millipore Sigma) unless indicated otherwise.

Osteogenic differentiation assay.

For differentiation assays, 10mM of β-glycerophosphate and 50μg/ml of ascorbic acid were

supplemented to culture medium. At indicated time points, matrix mineralization and collagen production were analyzed by Alizarin Red and Sirius Red staining respectively. Briefly, cells were fixed with ice-cold methanol and stained for 30' with 40mM Alizarin Red S solution (pH 4.2) (Sigma) or with a Sirius Red staining kit according to the manufacturers protocol (Abcam, ab150681). For quantification of the Alizarin Red staining, 1% cetylpyridinium chloride (CPC) in 10mM sodium phosphate, pH 7.0, was added to the wells for 15 min at room temperature on a tilting table. The extracted Alizarin Red solution was transferred to a 96 well plate along with an Alizarin Red standard curve (starting with a 1:50 dilution that accounts for 64.128 mg of calcium and followed by 1:2 dilutions) and absorbance was measured at 562 nm. The density-distance plot and pixel intensities were calculated with ImageJ software. For quantification of the Sirius Red staining, 1M NaOH was added to dissolute staining from the plate and absorbance was measured at 570 nm. Human calvarial osteoblasts (ScienCell) were cultured in commercially available osteoblast medium (ScienCell) and differentiated for 3 weeks using 10mM of β-glycerophosphate, 50 μg/ml of ascorbic acid and 10 nM dexamethasone.

Cell metabolism studies

Glucose levels in the conditioned medium were measured with a Contour glucose monitor and strips. ATP production was quantified by using the commercially available ATPLite kit (PerkinElmer). Oxygen consumption rate (OCR) and extracellular acidification rate (ECAR) were measured by Seahorse XFe96 extracellular flux analyzer (Agilent). Cells were seeded at a density of 60,000 cells/cm^2 in Seahorse XF96 microplates and differentiated for 3 weeks. OCR and ECAR were assessed during baseline conditions and after administrating mitochondrial stress test components (oligomycin (1 μM), carbonyl cyanide-p-trifluoromethoxyphenylhydrazone (FCCP) (1 μM), and rotenone (1 μM) along with antimycin A (1 μM)). Zinc uptake was measured on 2 and 3 weeks differentiated pCOBs using a commercial kit and according to the manufacturers protocol (Abcam) and using and EDTA-free lysis buffer. PFK activity was measured on 2 weeks differentiated pCOBs

using a commercial kit and procedures were followed according to the manufacturers protocol (Biovision).

Metabolomics

pCOBs were differentiated for 1 week in standard osteogenic medium and further differentiated in glucose-free DMEM with 10% dialyzed FBS (Thermofisher) and 1% pen/strep supplemented with $^{13}C_6$ glucose (Cambridge isotopes) during the second week. At the end of week two, cells were stopped and harvested with a mixture of methanol and dH_2O in an 80:20 ratio. After vortexing for 1 minute and sonication, samples were frozen in liquid N_2, thawed and centrifuged for 10 min at 14 000rpm. Supernatants, containing the intracellular metabolites, were stored at -80°C and the remaining pellets containing the mineralized matrix were treated with 1N HCl at 60°C for one hour with regular vortexing to free the mineral bound citrate. Subsequently samples were centrifuged for 10 min at 14 000rpm and supernatants were transferred to a new tube for HCl evaporation, resuspension in dH_2O and deproteination through 3kDa spin columns. The flow through was mixed with an equal volume of ice-cold acetonitrile for mass spectrometry analysis at the Johns Hopkins Metabolomics Facility. Metabolites were identified and quantified using Thermo-Scientific Q Exactive Plus Orbitrap mass spectrometer with Vanquish Horizon Binary UPLC. Data was analyzed using XCalibur, Compound Discoverer and TraceFinder software packages. Metabolites were identified using in-house compound standard databases as well as using MS/MS fragmentation data under identical conditions. Results were normalized to protein concentration for final results.

Radioactive tracer studies

For ^{14}C-Citrate uptake essays, pCOBs were seeded in 12 well plates and differentiated for indicated time periods. pCOBs were incubated with 5 μM ^{14}C-Citrate (Moravek) in Hank's balanced salt solution for 2hours at 37°C. After washing with ice-cold uptake buffer, pCOBs were lysed with 1% Triton in PBS to release the intracellular ^{14}C-Citrate. Radioactivity was measure by liquid scintillation.

RNA isolation and qRT-PCR

For RNA extraction, cells were lysed by adding RLT buffer (Qiagen) and RNA was extracted with the RNeasy microkit (Qiagen) according to the manufacturer's protocol. Tissues were homogenized in Trizol and RNA was extracted with chloroform and the RNeasy minikit (Qiagen). cDNA was synthesized from 1 µg RNA by incubation with iScript cDNA synthesis kit (Bio-Rad). For gene expression analysis, reactions were performed by combining iQ SYBR Green Supermix (Bio-Rad) with primers, which were derived from Harvard primer bank and shown in Supplementary Table 1. Gene expression levels were measured on a Biorad Real-Time PCR system (Bio-Rad) according to standard protocols with 18S as housekeeping gene. Expression levels were calculated using the ΔΔCt method.

Protein isolation and Western blot

For protein extraction from pCOBs, 150 µl transmembrane protein extraction reagent (FIVEphoton Biochemicals) supplemented with phenylmethylsulfonyl fluoride (PMSF, Millipore Sigma), Phosphatase inhibitor cocktail (Millipore Sigma) and protease inhibitor cocktail (Millipore Sigma) was added per 6-well. The cell extract was kept on ice for 2 hours with gentle vortex every 15 min and subsequently centrifuged for 30 min on 14,000 rpm at 4°C. Proteins from bones were isolated using the Minute™ Total Protein Extraction Kit for Bone Tissue (Invent Biotechnologies) according to the manufacturer's protocol. The denaturing lysis buffer was supplemented with Phosphatase inhibitor cocktail (Millipore Sigma), protease inhibitor cocktail (Millipore Sigma) and PMSF. Protein concentration was determined by the Pierce BCA Protein Assay kit (Thermofischer Scientiefic) and samples were prepared for immunoblotting according to standard techniques. Membranes were blocked with milk and primary antibodies were used in a 1:1000 concentration while HRP-conjugated secondary antibodies were used in a concentration of 1:3000. Blots were visualized using a chemiluminescent kit (SuperSignal West Femto, Thermo Scientific).

Supplemental Methods table 1: Reagents used in this study

Reagent or Resource	Source	Identifier
Antibodies		
β-Actin (8H10D10) Mouse mAb	Cell Signaling	3700
Anti-mouse IgG, HRP-linked Antibody	Cell Signaling	7076
Anti-rabbit IgG, HRP-linked Antibody	Cell signaling	7074
Acetyl-CoA Carboxylase (C83B10)	Cell signaling	3676
Phospho-Acetyl-CoA Carboxylase (Ser79) (D7D11)	Cell signaling	11818
AMPKα (D5A2) Rabbit mAb	Cell Signaling	5831
ACO2 (D6D9) XP® Rabbit mAb	Cell Signaling	6571
Phospho-AMPKα (Thr172) (40H9) Rabbit mAb	Cell Signaling	2535
Zip1	Santa Cruz	sc-393345
Slc13a5	Invitrogen	PA5-113058
Phospho-S6 Ribosomal Protein (Ser235/236)	Cell Signaling	4858
Phospho-S6 Ribosomal Protein (Ser240/244)	Cell Signaling	5364
Phospho-eIF4B (Ser422)	Cell Signaling	3591
p70 S6 Kinase (49D7)	Cell Signaling	2708
mTOR (7C10)	Cell Signaling	2983
GβL (86B8)	Cell Signaling	3274
Phospho-mTOR (Ser2448)	Cell Signaling	5536
Metabolites and inhibitors		
D-GLUCOSE (U-13C6, 99%)	Cambridge Isotope Laboratories	CLM-1396-PK
CITRIC ACID (13C6, 99%)	Cambridge Isotope Laboratories	CLM-9021-PK
PF-06761281	Millipore Sigma	PZ0318
Critical commercial assays and kits		
Citrate assay kit	Millipore Sigma	MAK057
Zinc assay kit	Abcam	ab102507
Phosphofructokinase (PFK) Activity Colorimetric Assay Kit	Biovision	K776
Agilent Seahorse XF Mito Stress test kit	Agilent	103015-100
Agilent Seahorse XF Calibrant solution	Agilent	100840-000
Agilent Seahorse XF RPMI medium	Agilent	103576-100
Agilent Seahorse XF sensor cartridges and cell culture microplates	Agilent	101085-004
VECTASTAIN® Elite® ABC-HRP Kit, Peroxidase (Rabbit IgG)	VectorLaboratories	PK6101
AEC Peroxidase (HRP) Substrate kit	LSBio	LS-J1076
Minute™ Total Protein Extraction Kit for Bone Tissue	Invent Biotechnologies	SA-02-BT
qPCR primers		

Alpl	PrimerBank (Massachusetts General Hospital)	PrimerBank ID: 6671533a1
Ank	PrimerBank (Massachusetts General Hospital)	PrimerBank ID: 31560341a1
Ctsk	PrimerBank (Massachusetts General Hospital)	PrimerBank ID: 142352209c1
Dmp1	PrimerBank (Massachusetts General Hospital)	PrimerBank ID: 33469121a1
Dspp	PrimerBank (Massachusetts General Hospital)	PrimerBank ID: 6753682a1
Enpp1	PrimerBank (Massachusetts General Hospital)	PrimerBank ID: 12597623a1
Ibsp	PrimerBank (Massachusetts General Hospital)	PrimerBank ID: 6680335a1
Mepe	PrimerBank (Massachusetts General Hospital)	PrimerBank ID: 16716459a1
Ocn	PrimerBank (Massachusetts General Hospital)	PrimerBank ID: 13811695a1
Opg	PrimerBank (Massachusetts General Hospital)	PrimerBank ID: 113930715c1
Opn	PrimerBank (Massachusetts General Hospital)	PrimerBank ID: 323668334c1
Rank	PrimerBank (Massachusetts General Hospital)	PrimerBank ID: 31981958a1
Rankl	PrimerBank (Massachusetts General Hospital)	PrimerBank ID: 6755833a1
Slc13a5	PrimerBank (Massachusetts General Hospital)	PrimerBank ID: 281306805c1
Slc13a3	PrimerBank (Massachusetts General Hospital)	PrimerBank ID: 16905091a1
Slc20a1/PiT	PrimerBank (Massachusetts General Hospital)	PrimerBank ID: 7657579a1
Slc25a1	PrimerBank (Massachusetts General Hospital)	PrimerBank ID: 23943838a1
Sost	PrimerBank (Massachusetts General Hospital)	PrimerBank ID: 14209688a1
Trap	PrimerBank (Massachusetts General Hospital)	PrimerBank ID: 6680624a1
Zip1 FW	5'-AGGTCAGGTGCTAACCATGAA-3'	
Zip1 RV	5'-CTGTTCCTTGTAAGCCAGCGT-3'	
18S	5'-CTTAGAGGGACAAGTGGCG-3'	
18S	5'-ACGCTGAGCCAGTCAGTGTA-3'	
Human GAPDH	PrimerBank (Massachusetts General Hospital)	PrimerBank ID: 378404907c1
Human SLC13A5	PrimerBank (Massachusetts General Hospital)	PrimerBank ID: 219802231c1

SI Appendix Figures and Figure legends

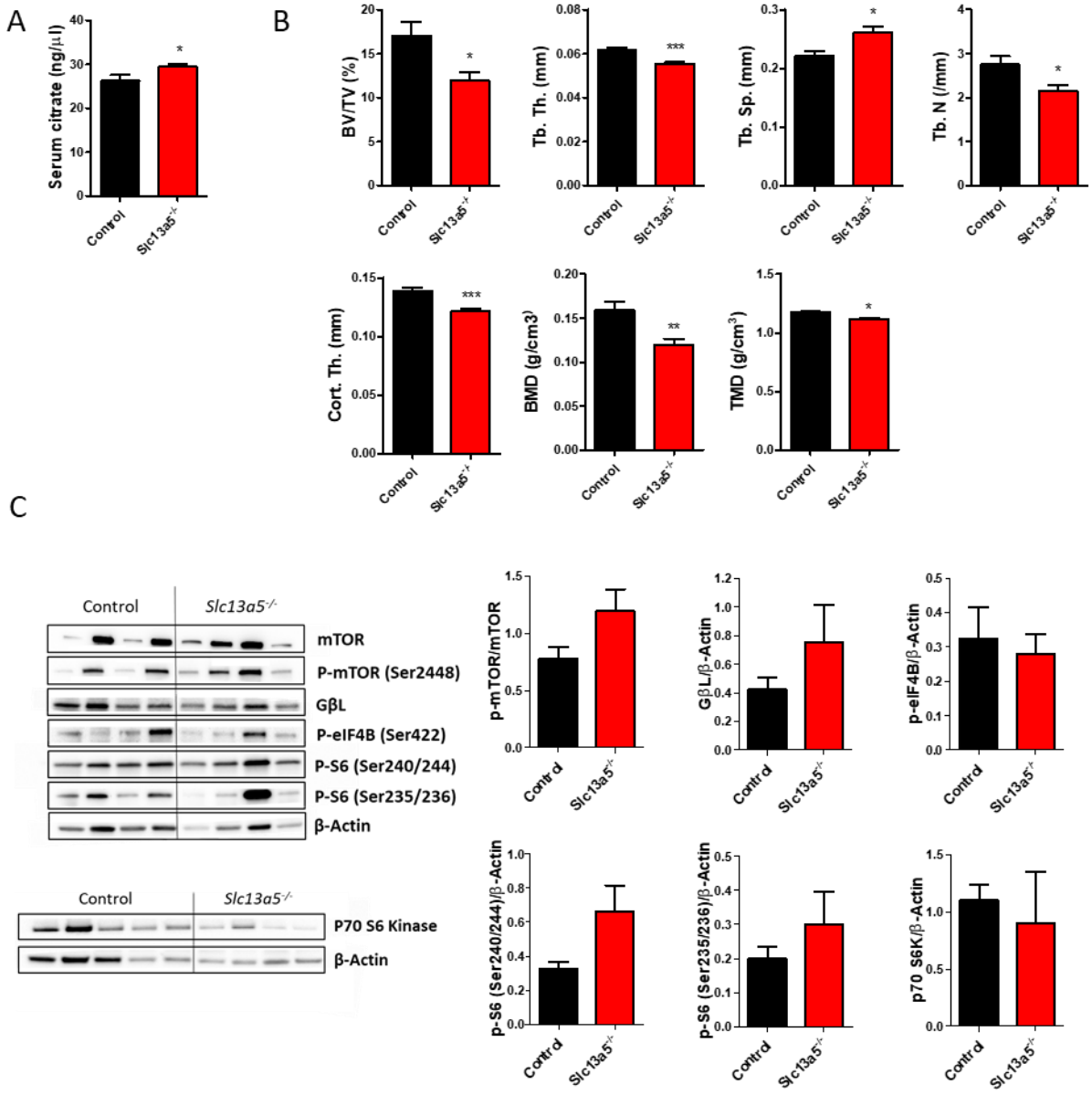

Fig. S1. Global *Slc13a5* deletion leads to high serum citrate levels and low bone mass without affecting protein synthesis**.** *(A)* Serum citrate levels in 6 week old female control and *Slc13a5*$^{-/-}$ mice (n=9-10). *(B)* Micro-CT analysis of the femur in 6 week old female control and *Slc13a5*$^{-/-}$ mice showing BV/TV%, Tb. Th., Tb. Sp., Tb. N., Cort. Th., BMD, TMD (n=7-8). *(C)* Western blot and quantification of mammalian target of rapamycin (mTOR) signaling, phosphorylated (P)-mTOR, GβL,

phosphorylated eukaryotic initiation factor 4B (P-eIF4B), phosphorylated (P)-S6 Ribosomal Protein, and p70 S6 Kinase in control and *Slc13a5*$^{-/-}$ mouse full bone lysates (n=4-5).

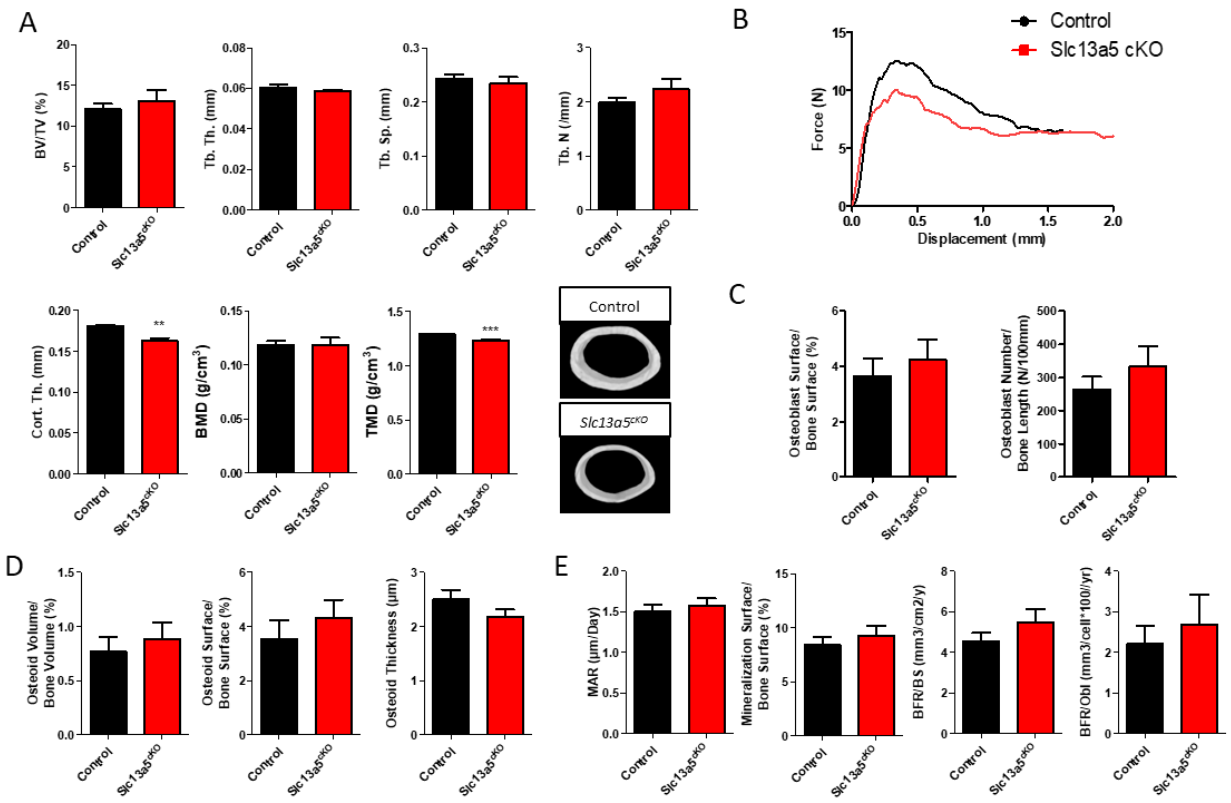

Fig. S2. Skeletal-specific *Slc13a5* deletion leads to low bone mass without affecting osteoblast parameters**.** *(A)* Micro-CT analysis of the femur in 10 week old female control and *Slc13a5*^{cKO} mice showing BV/TV%, Tb. Th., Tb. Sp., Tb. N., Cort. Th and representative 3D reconstruction of cortical bone (n=6-8). *(D)* Representative force-displacement curves derived from 3PB mechanical testing in control and *Slc13a5*^{cKO} mice (n=7-10). *(E)* Histomorphometry data showing Osteoblast Surface (left) and number (right) normalized for bone surface and length (n=10-12). *(F)* Histomorphometry data showing normalized osteoid volume (left), surface (middle) and thickness (right) (control and *Slc13a5*^{cKO}, n=10-12). *(G)* Dynamic histomorphometry data; MAR, mineral apposition rate; BFR/BS, bone formation rate over bone surface; BFR/Ob, bone formation rate per osteoblast (control and *Slc13a5*^{cKO}, n=10-12). All graphs represent mean ± SEM; Student's t-test versus control, **p<0.01, ***p<0.001

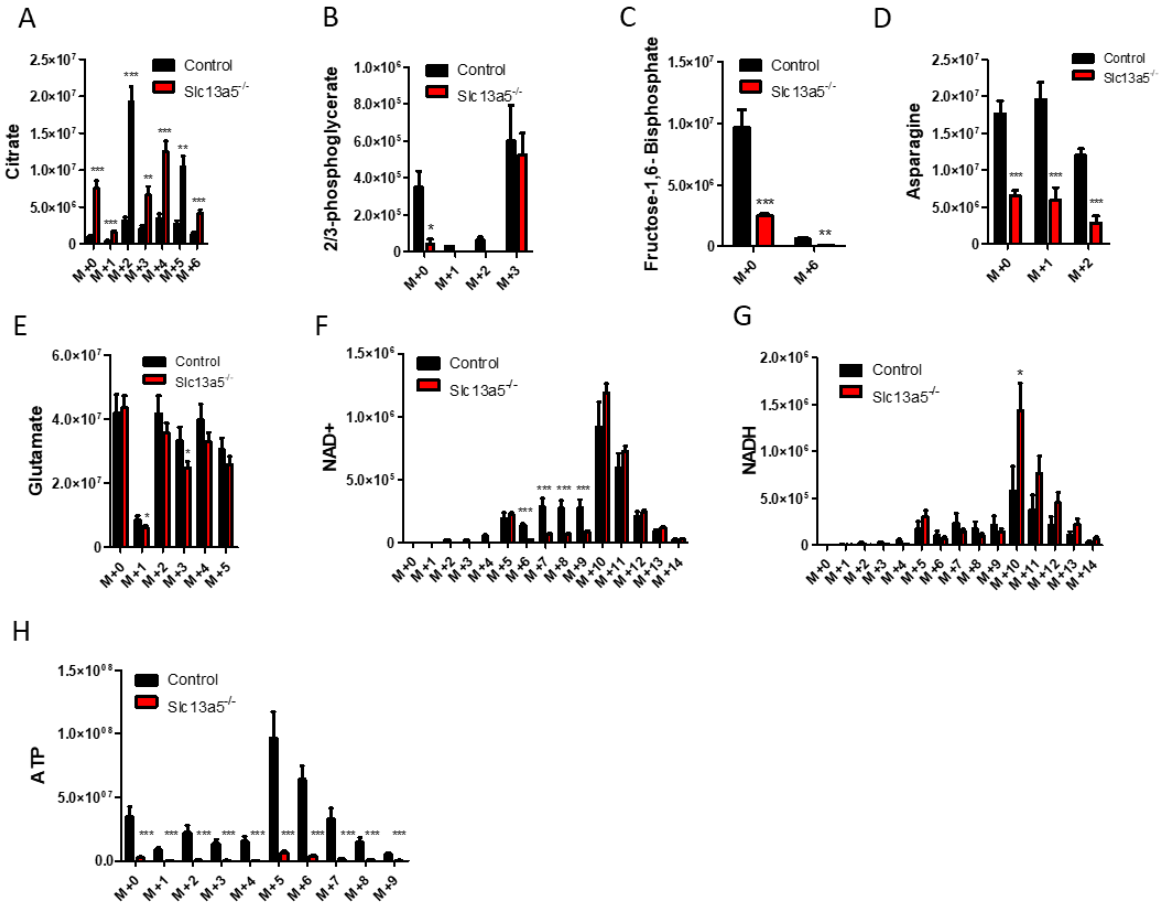

Fig. S3. *Slc13a5* deletion in osteoblasts depletes glycolytic metabolites and anaplerotic amino acids by diverting citrate from the TCA cycle. *(A)* Abundance of ^{13}C-labeled intracellular citrate derived from $^{13}C_6$-glucose normalized to cellular protein in differentiated control versus *Slc13a5*$^{-/-}$ pCOBs (n=4-5). *(B)* Abundance of ^{13}C-labeled intracellular 2/3-phosphoglycerate derived from $^{13}C_6$-glucose normalized to cellular protein in differentiated control versus *Slc13a5*$^{-/-}$ pCOBs (n=4-5). *(C)* Abundance of ^{13}C-labeled intracellular fructose-1,6-bisphosphate derived from $^{13}C_6$-glucose normalized to cellular protein in differentiated control versus *Slc13a5*$^{-/-}$ pCOBs (n=4-5). *(D)* Abundance of ^{13}C-labeled intracellular asparagine derived from $^{13}C_6$-glucose normalized to cellular protein in differentiated control versus *Slc13a5*$^{-/-}$ pCOBs (n=4-5). *(E)* Abundance of ^{13}C-labeled intracellular glutamate derived from $^{13}C_6$-glucose normalized to cellular protein in differentiated control versus *Slc13a5*$^{-/-}$ pCOBs (n=4-5). *(F)* NAD+ levels in differentiated control versus *Slc13a5*$^{-/-}$

pCOBs derived from metabolic flux analysis (n=4-5). *(G)* NADH levels in differentiated control versus *Slc13a5*$^{-/-}$ pCOBs derived from metabolic flux analysis (n=4-5). *(H)* ATP levels in differentiated control versus *Slc13a5*$^{-/-}$ pCOBs derived from metabolic flux analysis (n=4-5). All graphs represent mean ± SEM; Student's t-test versus control, *p<0.05, **p<0.01, ***p<0.001.

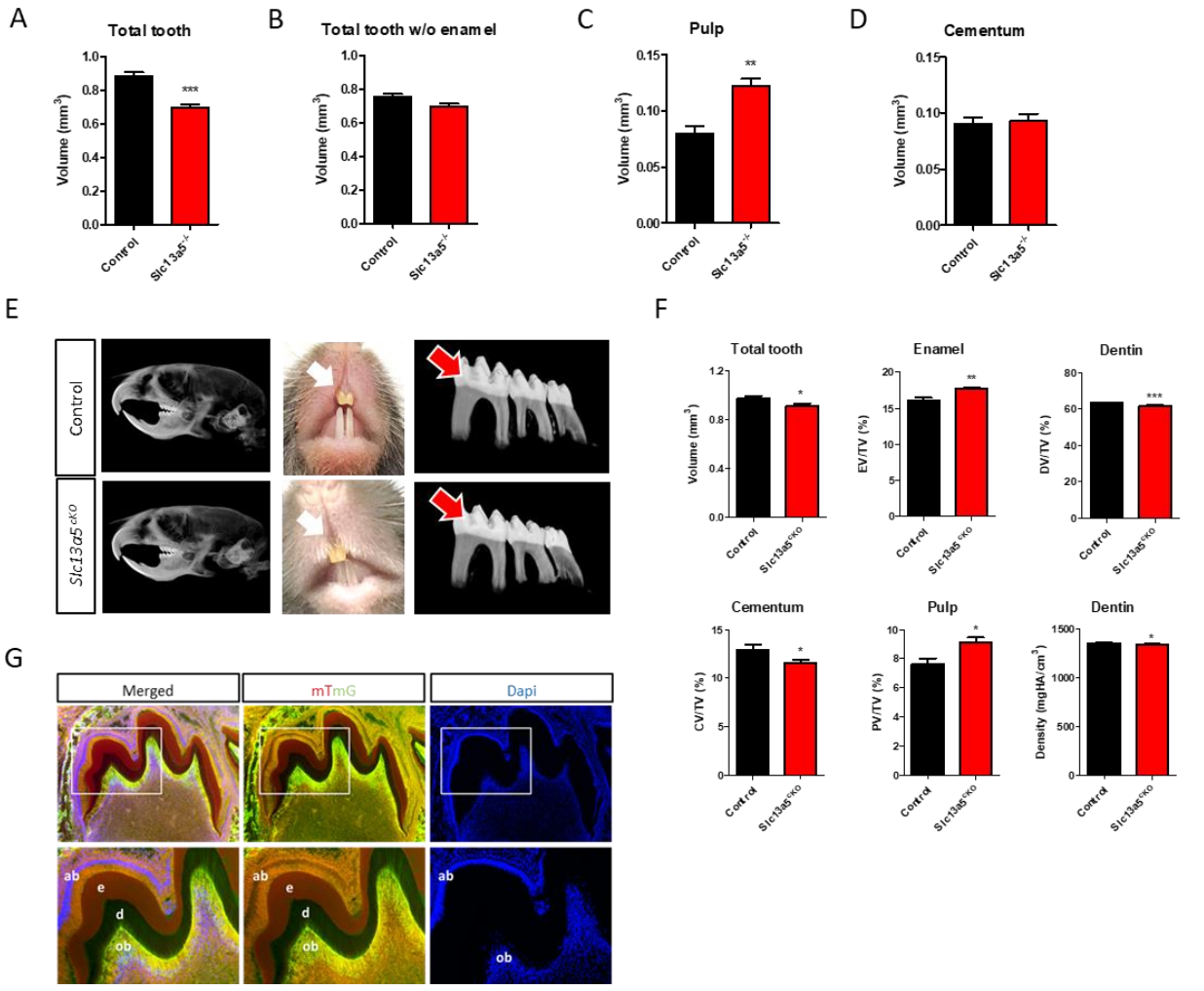

Fig. S4. Skeletal-specific *Slc13a5* deletion affects tooth volume and dentin mineralization. *(A)* 3D segmentation analysis showing total tooth volume (n=5). *(B)* 3D segmentation analysis showing tooth volume without enamel (n=5). *(C)* 3D segmentation analysis showing pulp volume (n=5). *(D)* 3D segmentation analysis showing cementum volume (n=5). *(E)* Representative image of control and *Slc13a5*^{cKO} mouse teeth without apparent alterations in tooth enamel in the mutants. *(F)* 3D segmentation analysis showing total tooth volume, enamel volume, dentin volume, cementum volume and pulp volume normalized for tooth volume and dentin density (n=9). *(G)* Representative image of *Ocn-Cre;mTmG* mouse teeth showing efficient recombination in odontoblasts (ob, GFP) and no recombination of the mTmG reporter in the ameloblasts (ab, Tomato). e, enamel; d, dentin. All graphs represent mean ± SEM; Student's t-test versus control, *p<0.05, **p<0.01, ***p<0.001.

References

1. Birkenfeld AL, Lee HY, Guebre-Egziabher F, Alves TC, Jurczak MJ, Jornayvaz FR, Zhang D, Hsiao JJ, Martin-Montalvo A, Fischer-Rosinsky A, Spranger J, Pfeiffer AF, Jordan J, Fromm MF, König J, Lieske S, Carmean CM, Frederick DW, Weismann D, et al. Deletion of the mammalian INDY homolog mimics aspects of dietary restriction and protects against adiposity and insulin resistance in mice. *Cell Metab*. 2011;14(2):184-195.
2. Zhang M, Xuan S, Bouxsein ML, Von Stechow D, Akeno N, Faugere MC, Malluche H, Zhao G, Rosen CJ, Efstratiadis A, Clemens TL. Osteoblast-specific knockout of the insulin-like growth factor (IGF) receptor gene reveals an essential role of IGF signaling in bone matrix mineralization. *J Biol Chem*. 2002;277(46):44005-44012.
3. Fedorov A, Beichel R, Kalpathy-Cramer J, Finet J, Fillion-Robin JC, Pujol S, Bauer C, Jennings D, Fennessy F, Sonka M, Buatti J, Aylward S, Miller J V., Pieper S, Kikinis R. 3D Slicer as an image computing platform for the Quantitative Imaging Network. *Magn Reson Imaging*. 2012;30(9):1323-1341.
4. Dempster DW, Compston JE, Drezner MK, Glorieux FH, Kanis JA, Malluche H, Meunier PJ, Ott SM, Recker RR, Parfitt AM. Standardized nomenclature, symbols, and units for bone histomorphometry: A 2012 update of the report of the ASBMR Histomorphometry Nomenclature Committee. *J Bone Miner Res*. 2013;28(1):2-17.